

Unconventional Magneto-Optical Effects in Altermagnets

Yongpan Li^{a,1}, Yichen Liu^{a,1}, and Cheng-Cheng Liu^{a,2}

This manuscript was compiled on December 4, 2025

The ideal altermagnets are a class of collinear, crystal-symmetry-enforced fully compensated magnets with nonrelativistic spin-split bands, in which contributions from Berry curvature to magneto-optical effects (MOEs) are strictly forbidden by an effective time-reversal symmetry. Here we show that, in such systems, MOEs are exclusively induced by the quantum metric and, in realistic altermagnets, are typically dominated by it. We refer to Berry-curvature-induced MOEs as conventional MOEs and to quantum-metric-dominated MOEs as unconventional MOEs. We derive general formulas that incorporate both Berry curvature and quantum metric for unconventional MOEs in altermagnets, enabling a quantitative evaluation of their respective contributions. Through symmetry analysis, we prove that ideal altermagnets are constrained to exhibit only unconventional MOEs. Using the three-dimensional canonical altermagnet MnTe and the emerging two-dimensional bilayer twisted altermagnet CrSBr as illustrative examples, we demonstrate that unconventional MOEs are prevalent in altermagnets. Our results establish altermagnets as a natural platform for quantum-metric-driven optical phenomena, substantially broadening the scope of MOEs and providing concrete predictions that can be tested in future experimental studies.

Unconventional Magneto-optical effect | Quantum geometry | Altermagnets

Riemannian geometry has deep connections with condensed matter physics (1–4), as the geometry of quantum states provides a powerful framework for understanding a wide range of response phenomena (5–13). Among these, magneto-optical effects (MOEs) have attracted particular attention (14–28). The central physical quantity underlying MOEs is the optical conductivity. Only recently has a comprehensive understanding of optical conductivity emerged from the perspective of topology and geometry, in terms of quantum geometry (9, 29, 30). However, conventional MOE theory accounts only for the imaginary part of quantum geometry, namely the Berry curvature, and largely overlooks the role of the real part, the quantum metric (31–34).

Ideal altermagnets possess an effective time-reversal symmetry—time-reversal combined with spin flipping—stemming from their intrinsically nonrelativistic character, i.e., the absence of spin-orbit coupling (SOC) (35–43). This effective time-reversal symmetry forbids the Berry curvature contribution to MOEs, rendering altermagnets seemingly trivial from the perspective of traditional MOE theory.

Here, we take an important step toward a complete understanding of MOEs in altermagnets. We first show that, strictly speaking, conventional MOE theory is valid only for systems with high (three-fold or higher) rotational symmetry. In such systems, contributions from the quantum metric to MOEs are forbidden, and the Berry curvature provides the sole source of MOEs. We refer to these Berry-curvature-induced responses as conventional MOEs. For the first time, we develop generic formulas for MOEs in altermagnets that explicitly incorporate both the quantum metric and Berry curvature, and we find that their contributions are coupled rather than simply additive. Through symmetry analysis, we prove that many ideal altermagnets support quantum-metric-induced MOEs. We term MOEs that are dominated by the quantum metric unconventional MOEs, i.e., cases in which the quantum metric contribution far exceeds that of the Berry curvature. Using our generic formulas in combination with first-principles calculations, we quantitatively calculate the Berry curvature and quantum metric contributions to MOEs and demonstrate the emergence of unconventional MOEs in altermagnets with SOC, using the three-dimensional (3D) canonical altermagnet MnTe and the emerging two-dimensional (2D) twisted bilayer altermagnet CrSBr as illustrative examples.

Significance Statement

The conventional view is that magneto-optical effects (MOEs) are driven exclusively by Berry curvature, implying that ideal altermagnets with effective time-reversal symmetry should be magneto-optically inactive. Here, we overturn this understanding by identifying a new mechanism for MOEs: quantum metric-induced or -dominated responses, which we term unconventional MOEs. Furthermore, we derive general formulas that incorporate both Berry curvature and quantum metric for unconventional MOEs in altermagnets, enabling a quantitative evaluation of their respective contributions. Using symmetry analysis and first-principles calculations, we demonstrate that such unconventional MOEs occur in both ideal and realistic altermagnets. Our work not only establishes a correct and unified theory of MOEs in altermagnets, but also opens a new direction for exploring quantum geometry driven magneto-optical phenomena.

Author affiliations: ^aCentre for Quantum Physics, Key Laboratory of Advanced Optoelectronic Quantum Architecture and Measurement (MOE), School of Physics, Beijing Institute of Technology, Beijing 100081, China

Author contributions: Cheng-Cheng Liu initiated the idea. Yongpan Li and Yichen Liu carried out DFT calculations and formula deduction. All authors contributed to the interpretation and analysis of the data. Yongpan Li, Yichen Liu, and Cheng-Cheng Liu wrote the manuscript.

The authors declare no conflict of interest.

¹ Yongpan Li and Yichen Liu contributed equally to this work.

² E-mail: ccliu@bit.edu.cn

Results and Discussion

Generic formulas for unconventional MOEs. The optical conductivity tensor σ is given by (9, 44)

$$\sigma_{ab}(\omega') = \frac{ie^2}{\hbar} \sum_{n \neq m} \int_{\mathbf{k}} \frac{f_{nm\mathbf{k}} \omega_{nm\mathbf{k}}}{\omega_{m\mathbf{k}} - \omega'} \left(g_{nm\mathbf{k}}^{ab} - \frac{i}{2} \Omega_{nm\mathbf{k}}^{ab} \right). \quad [1]$$

where $\int_{\mathbf{k}} \equiv \int d\mathbf{k}/(2\pi)^d$ with d the system dimension, a and b the cartesian coordinates, $f_{nm\mathbf{k}} \equiv f_{n\mathbf{k}} - f_{m\mathbf{k}}$ with $f_{n\mathbf{k}}$ the Fermi-Dirac distribution function, $\omega' \equiv \omega + i\eta$ with $\eta > 0$ the smearing parameter, and $\hbar\omega_{nm\mathbf{k}}$ the energy difference between the n th band and m th band. $g_{nm\mathbf{k}}^{ab}$ and $\Omega_{nm\mathbf{k}}^{ab}$ are the matrix elements of the quantum metric tensor \mathbf{g} and the Berry curvature tensor $\mathbf{\Omega}$ (i.e., the real and imaginary parts of the matrix elements of the quantum geometry tensor, respectively) and can be written as $g_{nm\mathbf{k}}^{ab} := (r_{nm\mathbf{k}}^a r_{mn\mathbf{k}}^b + r_{nm\mathbf{k}}^b r_{mn\mathbf{k}}^a)/2$ and $\Omega_{nm\mathbf{k}}^{ab} := i(r_{nm\mathbf{k}}^a r_{mn\mathbf{k}}^b - r_{nm\mathbf{k}}^b r_{mn\mathbf{k}}^a)$, where $r_{nm\mathbf{k}}^a$ are the matrix elements of the position operator.

While the longitudinal optical conductivities σ_{xx} and σ_{yy} are purely contributed by the quantum metric, the transverse optical conductivities σ_{xy} and σ_{yx} are contributed by both quantum metric and Berry curvature. Therefore, we divide the transverse optical conductivity σ_{ab} into the symmetric (σ_{ab}^g) and antisymmetric (σ_{ab}^Ω) parts, according to whether the contribution comes from the quantum metric g or the Berry curvature Ω . Then we have $\sigma_{xy} \equiv \sigma_{xy}^g + \sigma_{xy}^\Omega$ and $\sigma_{yx} \equiv \sigma_{yx}^g - \sigma_{yx}^\Omega$.

Consider a linearly polarized light incident normally on the surface of materials. Without loss of generality, we take the incident light propagates along the positive z -direction, i.e., $\mathbf{E} = E_0 e^{i(k_z z - \omega t)} \mathbf{x}$. By solving the wave equations in materials, the most general formulas for eigenmodes of light in the material, \mathbf{E}_\pm , and the corresponding complex refractive indices, n_\pm , read [Supplementary Information (SI) (45) Sec. I]

$$\mathbf{E}_\pm = \left(\frac{1}{2} \pm \frac{\sigma_{xx} - \sigma_{yy}}{2G} \right) E_0 e^{i(k_z z - \omega t)} \mathbf{x} \pm \frac{\sigma_{xy}^g - \sigma_{xy}^\Omega}{G} E_0 e^{i(k_z z - \omega t)} \mathbf{y}, \quad [2]$$

$$n_\pm = \sqrt{1 - \frac{\sigma_{xx} + \sigma_{yy} \pm G}{2i\omega\epsilon_0}}, \quad [3]$$

where $G = \sqrt{(\sigma_{yy} - \sigma_{xx})^2 + 4(\sigma_{xy}^g)^2 - 4(\sigma_{xy}^\Omega)^2}$. k_z is the effective complex wave vector, i.e., the incident light attenuates as the propagation distance increases. The relation between k_z and n_\pm is given by $k_z = n_\pm k_0$ with k_0 the wave propagation number in the vacuum, whose dielectric constant is ϵ_0 .

We derive generic formulas for the Kerr angle $\tilde{\theta}_K = \theta_K + i\xi_K$ and the Faraday angle $\tilde{\theta}_F = \theta_F + i\xi_F$ [SI (45) Sec. I]

$$\tilde{\theta}_K = \frac{2(\sigma_{xy}^g - \sigma_{xy}^\Omega)}{\sigma_{xx} - \sigma_{yy} + GR}, \quad [4]$$

$$\tilde{\theta}_F = \frac{2(\sigma_{xy}^g - \sigma_{xy}^\Omega)}{\sigma_{xx} - \sigma_{yy} + GT}. \quad [5]$$

Here, R^{-1} and T^{-1} are the reflection contrast ratio and transmission contrast ratio of the eigenmodes of light, respectively. For 3D systems, R and T are given by

$$R^{3D} = \frac{n_+ n_- - 1}{n_+ - n_-}, \quad T^{3D} = \frac{e^{ik_0 n_+ l} + e^{ik_0 n_- l}}{e^{ik_0 n_+ l} - e^{ik_0 n_- l}}, \quad [6]$$

where l is the propagation distance of the light. For 2D systems, R and T read

$$R^{2D} = \frac{r(n_+) + r(n_-)}{r(n_+) - r(n_-)}, \quad T^{2D} = \frac{t(n_+) + t(n_-)}{t(n_+) - t(n_-)}, \quad [7]$$

where $t(n_i)$ and $r(n_i)$ are the total complex transmission coefficient and the total complex reflection coefficient, respectively. The explicit expressions for $t(n_i)$ and $r(n_i)$ are given in SI (45) Sec. I.

Before proceeding, we provide a brief comparison between the representative 3D Kerr angle formulas for conventional MOEs and for our proposed unconventional MOEs. Conventional MOEs require crystals possessing at least three-fold rotational symmetry, enforcing a gyrotropic optical conductivity tensor ($\sigma_{xx} = \sigma_{yy}$, $\sigma_{xy}^g = \sigma_{yx}^g = 0$, and $\sigma_{xy}^\Omega = -\sigma_{yx}^\Omega \neq 0$). Applying the gyrotropic optical conductivity tensor to Eq. (4) yields the well-known and commonly used 3D Kerr angle formulas, i.e., $\theta_K = -\sigma_{xy}^\Omega / (\sigma_{xx} \sqrt{1 + i\sigma_{xx}/\omega\epsilon_0})$ (15, 18, 20, 31, 46) (See SI (45) Sec. I for the detailed derivation). The key differences between the conventional MOEs and the unconventional MOEs are: 1. Vanishing Berry curvature ($\sigma_{xy}^\Omega = 0$) forces vanishing Kerr angle in conventional MOEs, while a finite Kerr angle can be generated in unconventional MOEs even with zero Berry curvature. 2. Conventional MOE theory exclusively apply to systems with three-fold or higher rotational symmetry, while unconventional MOE theory are applicable to systems of arbitrary symmetry.

Unconventional MOEs in altermagnets. An ideal altermagnet is a collinear and crystal-symmetry fully compensated magnet described by spin symmetry, whose Néel vector is odd under some real space symmetries other than inversion and translation symmetries (36–42, 48, 49). Because of the decoupling of the real space symmetry and spin space symmetry, ideal altermagnets always possess an effective time-reversal symmetry, i.e., a time-reversal symmetry combined with a spin inversion symmetry.

Under the effective time-reversal symmetry, the matrix elements of the Berry curvature tensor and the quantum metric tensor satisfy $\Omega_{nm\mathbf{k}}^{ab} = -\Omega_{nm, -\mathbf{k}}^{ab}$ and $g_{nm\mathbf{k}}^{ab} = g_{nm, -\mathbf{k}}^{ab}$. Therefore, the integral of the Berry curvature over the entire Brillouin zone (BZ) in Eq. (1) is zero, i.e., $\sigma_{xy}^\Omega = \sigma_{yx}^\Omega = 0$, and ideal altermagnets never show conventional MOEs. While the effective time-reversal symmetry does not lead to a vanishing integral of the quantum metric, the high rotational symmetry forbids the contribution of the quantum metric to the MOEs. Under high rotational symmetry, we have $\sigma_{xy}^g = -\sigma_{yx}^g$ and $\sigma_{xx} = \sigma_{yy}$. However, the matrix elements of the quantum metric tensor are symmetric under swapping of x and y , i.e., $g_{nm\mathbf{k}}^{xy} = g_{nm\mathbf{k}}^{yx}$ and $\sigma_{xy}^g = \sigma_{yx}^g = 0$. According to Eq. (3), the complex refractive indices for two eigenmodes are the same and there are no unconventional MOEs either.

While conventional MOEs are rigorously forbidden in ideal altermagnets and unconventional MOEs are prohibited by three-fold or higher rotational symmetry, a lot of altermagnets show unconventional MOEs. For 2D systems, there are many 2D altermagnets without high rotational symmetry, for example, the opposite-spin sublattices are connected by two-fold rotational symmetry. For 3D systems, even if an altermagnet possesses high rotational symmetry, not all of its cleavage planes have high rotational symmetry. As long

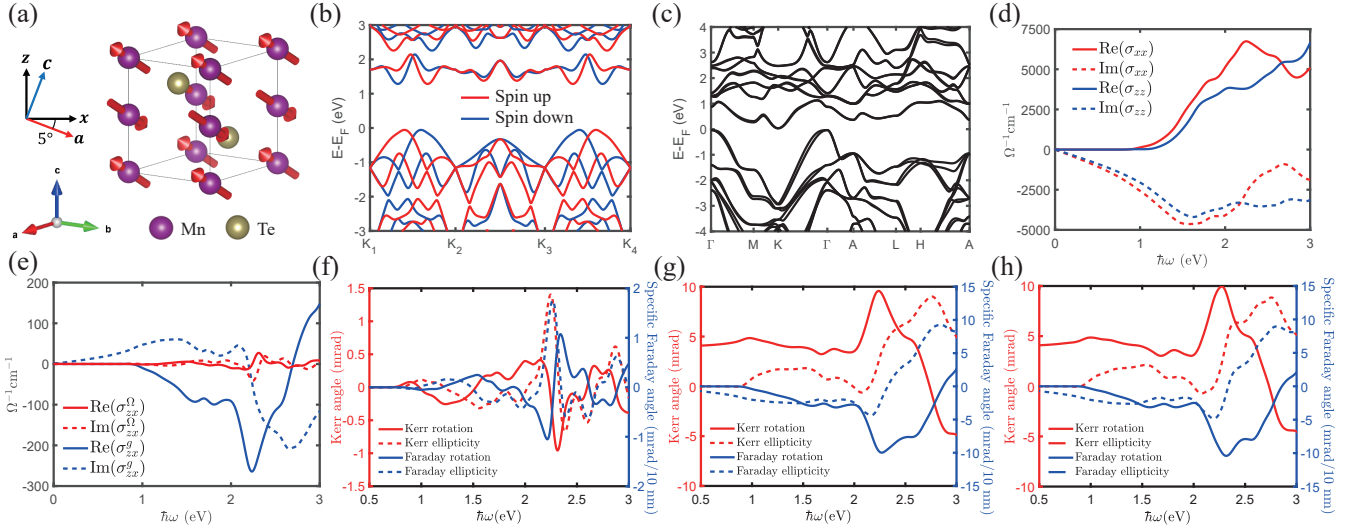


Fig. 1. The unconventional magneto-optical effects in 3D altermagnet MnTe. (a) The magnetic unit cell of MnTe, as drawn using VESTA (47). The polarization direction of the incident light lies within the ac plane, forming an angle of 5° with respect to the a -axis. (b) The DFT spin splitting band structure without SOC. The positions of the four momenta are given by $K_1 = (1/3, 1/3, 1/4)$, $K_2 = (1/3, -2/3, 1/4)$, $K_3 = (1/3, 1/3, -1/4)$, $K_4 = (1/3, -2/3, -1/4)$. (c) The DFT band structure with SOC. (d) The longitudinal optical conductivities σ_{xx} and σ_{zz} . (e) The transverse optical conductivities $\sigma_{zx} \equiv \sigma_{zx}^g + \sigma_{zx}^\Omega$. σ_{zx} is divided into the symmetric part σ_{zx}^g and the antisymmetric part σ_{zx}^Ω . (f) The calculated Kerr and specific Faraday angles when the Berry curvature exclusively contributes to the transverse optical conductivities. (g) The calculated Kerr and specific Faraday angles when the contribution comes exclusively from the quantum metric. (h) The Kerr angles and specific Faraday angles with the consideration of both the Berry curvature and quantum metric. The calculations in (d)–(h) have all incorporated SOC.

as the light is incident on a surface without high rotational symmetry, the unconventional MOEs are still present.

In real altermagnets, although SOC may be very small, it is always present, coupling the real-space symmetry and spin-space symmetry, thus preventing the existence of effective time-reversal symmetry. Even though altermagnets with SOC are capable of exhibiting conventional MOEs, we demonstrate in the following sections that unconventional MOEs, i.e., the quantum metric-dominated MOEs, can frequently emerge in real altermagnets. In the subsequent first-principles calculations of real altermagnets, the SOC is included and the corresponding symmetry group changes from the spin group to the magnetic group.

Unconventional MOEs in 3D altermagnet MnTe. MnTe has a NiAs-type structure with the space group $P6_3/mmc$ (No. 194) [Fig. 1(a)]. The antiferromagnetism of the MnTe has been confirmed by neutron diffraction experiments (50–52) and MnTe has a high bulk Néel temperature of 307 K (50, 52, 53). The opposite-spin sublattices are connected by C_{6z} combined with translation through $(0, 0, 1/2)$. Although the inversion symmetry is present, it connects two atoms with the same magnetic moment. MnTe has an anisotropic g -wave spin-splitting (54, 55) as shown in Fig. 1(b). The magnetic moments of MnTe can be tuned by an external magnetic field (56), and we take the magnetic moments to lie within the ac plane, forming an angle of 30° with respect to the a -axis as shown in Fig. 1(a). Then the magnetic space group of MnTe is $C2/c.1$ (No. 15.85) and the band structure is shown in Fig. 1(c).

In Figs. 1(d) and (e), the longitudinal and transverse optical conductivities are shown in the range of 0–3 eV, which falls within the energy range of conventional lasers. Here, we show the transverse optical conductivity σ_{zx} in terms of its symmetric (σ_{zx}^g) and antisymmetric (σ_{zx}^Ω) parts, where the

xz -axes are given by rotating the ac -axes by 5° as depicted in Fig. 1(a). One can find that the contribution of the quantum metric to the transverse optical conductivities is significantly greater than that of the Berry curvature.

The Kerr angle and specific Faraday angle, i.e., Faraday angle per unit thickness l with $l=10$ nm, are calculated in the range of 0.5–3 eV considering the respective contribution of the Berry curvature [Fig. 1(f)] and the quantum metric [Fig. 1(g)] to the transverse optical conductivities. For the Kerr effect, the maximum Kerr rotation and ellipticity are -0.96 mrad and 1.4 mrad, when considering exclusively the Berry curvature’s contribution to the transverse conductivities, and surge to 9.6 mrad and 9.0 mrad, when considering exclusively the quantum metric’s contribution. For the Faraday effect, the maximum specific Faraday rotation and ellipticity are 1.1 mrad/10 nm and 1.8 mrad/10 nm, when considering exclusively the Berry curvature’s contribution to the transverse conductivities, and are significantly increased to -10 mrad/10 nm and 9.3 mrad/10 nm, when considering exclusively the quantum metric’s contribution.

From Fig. 1(f) and Fig. 1(g), it can be observed that the contribution of the Berry curvature to the MOEs is much smaller compared to those induced solely by the quantum metric. In Fig. 1(h), we calculate the total Kerr angle and specific Faraday angle considering both the contributions of the quantum metric and the Berry curvature. Since the quantum metric dominates the contribution to MOEs, we find that the total Kerr angle and total Faraday angle are almost identical to those calculated without considering Berry curvature. Based on the above-detailed calculations, it follows that unconventional MOEs emerge in the 3D canonical altermagnet MnTe.

Unconventional MOEs in 2D altermagnet CrSBr. The bulk CrSBr is a layered van der Waals antiferromagnet with

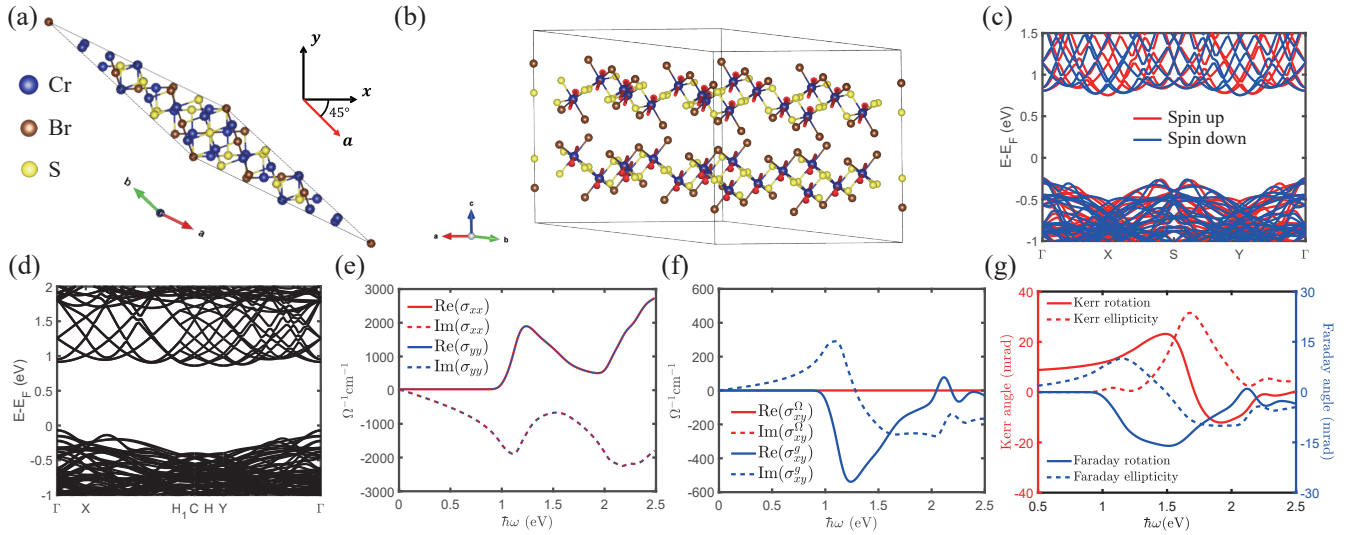


Fig. 2. The unconventional magneto-optical effects in 2D bilayer twisted altermagnet CrSBr. (a) Top view of the unit cell of the twisted bilayer CrSBr with a twist angle 73.44°. The polarization direction of the incident light lies within the ab plane, forming an angle of 45° with respect to the a -axis. (b) The magnetic unit cell of twisted bilayer CrSBr. (c) The DFT spin splitting band structure without SOC. (d) The DFT band structure with SOC. (e) The longitudinal optical conductivities σ_{xx} and σ_{yy} . (f) The transverse conductivities $\sigma_{xy} \equiv \sigma_{xy}^g + \sigma_{xy}^\Omega$. σ_{xy} is divided into symmetric part σ_{xy}^g and antisymmetric part σ_{xy}^Ω . (g) The Kerr angles and Faraday angles. Given that the Berry curvature does not contribute to the MOEs, we only present the total Kerr and Faraday angles. The calculations in (e)–(g) have all incorporated SOC.

interlayer antiferromagnetic order and intralayer ferromagnetic order (57–60) and has a bulk Néel temperature of 132 K (58, 59). The crystal structure of bulk CrSBr belongs to space group $Pm\bar{m}m$ (No. 59). The twisted bilayer CrSBr has been prepared experimentally (60). The twisted bilayer CrSBr with a twist angle 73.44° belonging to the space group $C222$ (No. 21) [Fig. 2(a) and Fig. 2(b)] is an altermagnet of d -wave (61, 62), as shown in Fig. 2(c). The twisted bilayer CrSBr has an in-plane Néel vector, and our qualitative conclusion (i.e., the twisted bilayer CrSBr shows unconventional MOEs) is independent of the specific direction of the in-plane Néel vector. Here, we take the Néel vector along the $\mathbf{a} + \mathbf{b}$ direction. Then the magnetic space group of CrSBr is $C22'2'$ (No. 21.41) and the band structure is shown in Fig. 2(d).

The longitudinal and transverse optical conductivities are shown in Fig. 2(e) and Fig. 2(f), respectively, with photon energy ranging from 0 to 2.5 eV. Due to the presence of $C_{2z}\mathcal{T}$, the contribution of the Berry curvature to the transverse optical conductivities is forbidden. As a result, the MOEs are contributed exclusively by the quantum metric in the twisted bilayer CrSBr, i.e., the twisted bilayer CrSBr shows unconventional MOEs. The Kerr and Faraday angles are calculated in the range of 0.5–2.5 eV as shown in Fig. 2(g). The quantum metric alone induces a remarkable Kerr angle in twisted bilayer CrSBr, with the maximum Kerr rotation and ellipticity reaching 23 mrad and 31 mrad, respectively. Meanwhile, in the Faraday effects, remarkable Faraday rotation and ellipticity of -16 mrad and 10 mrad are achieved.

Discussion. In traditional MOE theory, the polarization direction of the incident light—i.e., the orientation of its electric field—does not affect the magnitude of the MOE signal. By contrast, in MnTe and twisted bilayer CrSBr, we find that the MOE signal depends strongly on the polarization direction of the incident light (with the x direction taken

as the polarization axis in this work). This difference originates from the symmetry of the plane of incidence. In the traditional framework, the plane of incidence has high rotational symmetry, and the eigenmodes of light are left- and right-circularly polarized. Decomposing incident linearly polarized light into these circular eigenmodes always yields equal amplitudes, independent of the polarization direction. As a result, the Kerr and Faraday angles are the same for different linear polarization directions in the traditional theory. In the more general case where high rotational symmetry is absent, however, the eigenmodes become elliptically polarized [see Eq. (2)]. Decomposing linearly polarized light with different polarization directions into these elliptically polarized eigenmodes produces direction-dependent amplitude ratios. Consequently, linearly polarized light with different polarization directions gives rise to different Kerr or Faraday angles in the unconventional MOEs we propose.

In this work, the traditional understanding is challenged that MOEs are exclusively induced by Berry curvature. We show that the standard formulas for what we call conventional MOEs apply only to a limited subset of altermagnets with high rotational symmetry. We identify a new mechanism—quantum metric-induced or -dominated responses—that both deepens and broadens the conceptual framework of MOEs. Because our predictions can be tested using standard MOE experimental techniques, they provide a direct route to experimental validation. More broadly, our results highlight altermagnets as a promising platform for quantum-geometry-driven optical phenomena, with important implications for future magneto-optical applications and for stimulating further theoretical and experimental exploration.

ACKNOWLEDGMENTS. The work is supported by the NSF of China (Grant No. 12374055), the Science Fund for Creative Research Groups of NSFC (Grant No. 12321004), and the National Key R&D Program of China (Grant No. 2020YFA0308800).

1. JP Provost, G Vallee, Riemannian structure on manifolds of quantum states. *Commun.Math. Phys.* **76**, 289–301 (1980).
2. A Shapere, F Wilczek, *Geometric phases in physics*. (World scientific) Vol. 5, (1989).
3. YQ Ma, S Chen, H Fan, WM Liu, Abelian and non-Abelian quantum geometric tensor. *Phys. Rev. B* **81**, 245129 (2010).
4. T Liu, XB Qiang, HZ Lu, XC Xie, Quantum geometry in condensed matter. *Natl. Sci. Rev. p. nwae334* (2024).
5. N Nagaosa, J Sinova, S Onoda, AH MacDonald, NP Ong, Anomalous hall effect. *Rev. Mod. Phys.* **82**, 1539–1592 (2010).
6. Y Gao, SA Yang, Q Niu, Field Induced Positional Shift of Bloch Electrons and Its Dynamical Implications. *Phys. Rev. Lett.* **112**, 166601 (2014).
7. I Sodemann, L Fu, Quantum Nonlinear Hall Effect Induced by Berry Curvature Dipole in Time-Reversal Invariant Materials. *Phys. Rev. Lett.* **115**, 216806 (2015).
8. P Törmä, S Peotta, BA Bernevig, Superconductivity, superfluidity and quantum geometry in twisted multilayer systems. *Nat. Rev. Phys.* **4**, 528–542 (2022).
9. J Ahn, GY Guo, N Nagaosa, A Vishwanath, Riemannian geometry of resonant optical responses. *Nat. Phys.* **18**, 290–295 (2022).
10. D Kaplan, T Holder, B Yan, Unification of nonlinear anomalous hall effect and nonreciprocal magnetoresistance in metals by the quantum geometry. *Phys. Rev. Lett.* **132**, 026301 (2024).
11. N Verma, R Queiroz, Instantaneous response and quantum geometry of insulators. *arXiv:2403.07052* (2024).
12. M Ezawa, Analytic approach to quantum metric and optical conductivity in dirac models with parabolic mass in arbitrary dimensions. *arXiv:2408.02951* (2024).
13. Y Onishi, L Fu, Fundamental bound on topological gap. *Phys. Rev. X* **14**, 011052 (2024).
14. JL Erskine, EA Stern, Magneto-optic Kerr Effect in Ni, Co, and Fe. *Phys. Rev. Lett.* **30**, 1329–1332 (1973).
15. W Wetling, Magneto-optics of ferrites. *J. Magn. Magn. Mater.* **3**, 147–160 (1976).
16. T Kato, H Kikuzawa, S Iwata, S Tsunashima, S Uchiyama, Magneto-optical effect in MnPt₃ alloy films. *J. Magn. Magn. Mater.* **140-144**, 713–714 (1995).
17. GY Guo, H Ebert, Band-theoretical investigation of the magneto-optical Kerr effect in Fe and Co multilayers. *Phys. Rev. B* **51**, 12633–12643 (1995).
18. S Tomita, et al., Magneto-Optical Kerr Effects of Yttrium-Iron Garnet Thin Films Incorporating Gold Nanoparticles. *Phys. Rev. Lett.* **96**, 167402 (2006).
19. WK Tse, AH MacDonald, Giant Magneto-Optical Kerr Effect and Universal Faraday Effect in Thin-Film Topological Insulators. *Phys. Rev. Lett.* **105**, 057401 (2010).
20. W Feng, GY Guo, J Zhou, Y Yao, Q Niu, Large magneto-optical Kerr effect in noncollinear antiferromagnets Mn₃X (X = Rh, Ir, Pt). *Phys. Rev. B* **92**, 144426 (2015).
21. N Sivasdas, S Okamoto, D Xiao, Gate-Controllable Magneto-optic Kerr Effect in Layered Collinear Antiferromagnets. *Phys. Rev. Lett.* **117**, 267203 (2016).
22. B Huang, et al., Layer-dependent ferromagnetism in a van der waals crystal down to the monolayer limit. *Nature* **546**, 270–273 (2017).
23. J Ahn, SY Xu, A Vishwanath, Theory of optical axion electrodynamics and application to the Kerr effect in topological antiferromagnets. *Nat. Commun.* **13**, 7615 (2022).
24. I Lyalin, S Alikhah, M Berritta, PM Oppeneer, RK Kawakami, Magneto-Optical Detection of the Orbital Hall Effect in Chromium. *Phys. Rev. Lett.* **131**, 156702 (2023).
25. YD Kato, Y Okamura, M Hirschberger, Y Tokura, Y Takahashi, Topological magneto-optical effect from skyrmion lattice. *Nat. Commun.* **14**, 5416 (2023).
26. I Mazin, R González-Hernández, L Šmejkal, Induced monolayer altermagnetism in MnP(S, Se)₃ and FeSe. *arXiv:2309.02355* (2023).
27. X Li, et al., Topological Kerr effects in two-dimensional magnets with broken inversion symmetry. *Nat. Phys.* **20**, 1145–1151 (2024).
28. W Chen, X Zhou, WK Lou, K Chang, Magneto-optical conductivity and circular dichroism in *d*-wave altermagnets. *Phys. Rev. B* **111**, 064428 (2025).
29. I Komissarov, T Holder, R Queiroz, The quantum geometric origin of capacitance in insulators. *Nat. Commun.* **15**, 4621 (2024).
30. N Verma, R Queiroz, Instantaneous Response and Quantum Geometry of Insulators. *arXiv:2403.07052* (2024).
31. FJ Kahn, PS Pershan, JP Remeika, Ultraviolet Magneto-Optical Properties of Single-Crystal Orthoferrites, Garnets, and Other Ferric Oxide Compounds. *Phys. Rev.* **186**, 891–918 (1969).
32. W Voigt, *Magneto-und elektrooptik*. (BG Teubner) No. 3, (1908).
33. K.H.J. Buschow, E.P. Wohlfarth, *Handbook of Ferromagnetic Materials*. (North Holland), (1990).
34. W Kuch, R Schäfer, P Fischer, FU Hillebrecht, *Magnetic Microscopy of Layered Structures*. (Springer Berlin, Heidelberg), (2014).
35. C Wu, K Sun, E Fradkin, SC Zhang, Fermi liquid instabilities in the spin channel. *Phys. Rev. B* **75**, 115103 (2007).
36. LD Yuan, Z Wang, JW Luo, EI Rashba, A Zunger, Giant momentum-dependent spin splitting in centrosymmetric low-*z* antiferromagnets. *Phys. Rev. B* **102**, 014422 (2020).
37. R González-Hernández, et al., Efficient Electrical Spin Splitter Based on Nonrelativistic Collinear Antiferromagnetism. *Phys. Rev. Lett.* **126**, 127701 (2021).
38. HY Ma, et al., Multifunctional antiferromagnetic materials with giant piezomagnetism and noncollinear spin current. *Nat. Commun.* **12**, 2846 (2021).
39. L Šmejkal, J Sinova, T Jungwirth, Beyond Conventional Ferromagnetism and Antiferromagnetism: A Phase with Nonrelativistic Spin and Crystal Rotation Symmetry. *Phys. Rev. X* **12**, 031042 (2022).
40. L Šmejkal, J Sinova, T Jungwirth, Emerging Research Landscape of Altermagnetism. *Phys. Rev. X* **12**, 040501 (2022).
41. PA McClarty, JG Rau, Landau Theory of Altermagnetism. *Phys. Rev. Lett.* **132**, 176702 (2024).
42. L Bai, et al., Altermagnetism: Exploring new frontiers in magnetism and spintronics. *Adv. Funct. Mater.* **34**, 2409327 (2024).
43. I Mazin, Editorial: Altermagnetism—a new punch line of fundamental magnetism. *Phys. Rev. X* **12**, 040002 (2022).
44. C Aversa, JE Sipe, Nonlinear Optical Susceptibilities of Semiconductors: Results with a Length-Gauge Analysis. *Phys. Rev. B* **52**, 14636–14645 (1995).
45. See Supplemental Information for more detailed information on (I) Formulas for unconvention magneto-optical effects, (II) Calculation details, which includes Ref. (15, 18, 20, 33, 34, 44, 46, 63–72).
46. A Kirilyuk, AV Kimel, T Rasing, Ultrafast optical manipulation of magnetic order. *Rev. Mod. Phys.* **82**, 2731–2784 (2010).
47. K Momma, F Izumi, *VESTA* for three-dimensional visualization of crystal, volumetric and morphology data. *J. Appl. Crystallogr.* **44**, 1272–1276 (2011).
48. P Liu, J Li, J Han, X Wan, Q Liu, Spin-group symmetry in magnetic materials with negligible spin-orbit coupling. *Phys. Rev. X* **12**, 021016 (2022).
49. PJ Guo, ZX Liu, ZY Lu, Quantum anomalous hall effect in collinear antiferromagnetism. *npj Comput. Mater.* **9**, 70 (2023).
50. T Komatsubara, M Murakami, E Hirahara, Magnetic Properties of Manganese Telluride Single Crystals. *J. Phys. Soc. Jpn.* **18**, 356–364 (1963).
51. N Kunitomi, Y Hamaguchi, S Anzai, Neutron diffraction study on manganese telluride. *J. Phys. France* **25**, 568–574 (1964).
52. J Efreim D'Sa, et al., Low-temperature neutron diffraction study of MnTe. *J. Magn. Magn. Mater.* **285**, 267–271 (2005).
53. CF Squire, Antiferromagnetism in Some Manganous Compounds. *Phys. Rev.* **56**, 922–925 (1939).
54. J Krempaský, et al., Altermagnetic lifting of kramers spin degeneracy. *Nature* **626**, 517–522 (2024).
55. S Lee, et al., Broken Kramers Degeneracy in Altermagnetic MnTe. *Phys. Rev. Lett.* **132**, 036702 (2024).
56. RD Gonzalez Betancourt, et al., Spontaneous anomalous hall effect arising from an unconventional compensated magnetic phase in a semiconductor. *Phys. Rev. Lett.* **130**, 036702 (2023).
57. H Katscher, H Hahn, Über chalcogenidhalogenide des dreiwertigen chroms. *Naturwissenschaften* **53**, 361–361 (1966).
58. O Göser, W Paul, H Kahle, Magnetic properties of CrSBr. *J. Magn. Magn. Mater.* **92**, 129–136 (1990).
59. K Lee, et al., Magnetic Order and Symmetry in the 2D Semiconductor CrSBr. *Nano Lett.* **21**, 3511–3517 (2021).
60. J Klein, et al., Control of structure and spin texture in the van der Waals layered magnet CrSBr. *Nat. Commun.* **13**, 5420 (2022).
61. J Yu, S Qian, CC Liu, General Electronic Structure Calculation Method for Twisted Systems. *arXiv:2407.08110* (2024).
62. Y Liu, J Yu, CC Liu, Twisted magnetic van der waals bilayers: An ideal platform for altermagnetism. *Phys. Rev. Lett.* **133**, 206702 (2024).
63. LD Landau, EM Lifshitz, *Electrodynamics of Continuous Media*. (Pergamon Press), (1961).
64. PS Pershan, Magneto-optical effects. *J. Appl. Phys.* **38**, 1482–1490 (1967).
65. R Azzam, N Bashara, D Thorburn Burns, *Ellipsometry and polarized light*. (North-Holland, Amsterdam), (1987).
66. M Born, E Wolf, *Principles of optics: electromagnetic theory of propagation, interference and diffraction of light*. (Elsevier), (2013).
67. MH Kim, et al., Determination of the infrared complex magnetoconductivity tensor in itinerant ferromagnets from Faraday and Kerr measurements. *Phys. Rev. B* **75**, 214416 (2007).
68. G Kresse, J Furthmüller, Efficient iterative schemes for *ab initio* total-energy calculations using a plane-wave basis set. *Phys. Rev. B* **54**, 11169 (1996).
69. JP Perdew, K Burke, M Ernzerhof, Generalized gradient approximation made simple. *Phys. Rev. Lett.* **77**, 3865 (1996).
70. AA Mostofi, et al., wannier90: A tool for obtaining maximally-localised wannier functions. *Comput. Phys. Commun.* **178**, 685–699 (2008).
71. G Pizzi, et al., Wannier90 as a community code: New features and applications. *J. Phys.: Condens. Matter* **32**, 165902 (2020).
72. J Heyd, GE Scuseria, M Ernzerhof, Hybrid functionals based on a screened coulomb potential. *J. Chem. Phys.* **118**, 8207–8215 (2003).